Density Functional Study of Ethylene Polymerization Catalyzed by a Zirconium Non-Cyclopentadienyl Complex, $L_2ZrCH_3^+$. Effects of Ligands and Bulky Substituents

Sergei F. Vyboishchikov,† Djamaladdin G. Musaev,* Robert D. J. Froese, and Keiji Morokuma*

Cherry L. Emerson Center for Scientific Computation and Department of Chemistry, Emory University, Atlanta, Georgia 30322

Received August 14, 2000

To elucidate the role of electronic and steric effects on catalytic activities and to gain some guidance for the design of catalysts, we applied the hybrid density functional B3LYP and integrated molecular orbital + molecular mechanics (IMOMM) methods to study the mechanism of the chain initiation/propagation reaction of L_2ZrMe^+-catalyzed ethylene polymerization for several bidentate non-cyclopentadienyl ligands [L = −O−CH═CH−CH═NH− (**1** (*trans*), **2** (*cis*)), HCO_2 (**3**), $HC(NH)_2$ (**4**), HC(O)(NH) (**5** (*cis*), **6** (*trans*)), −O−CH═CH−N(CH_2) (**7**)], ^{t}Bu-**4** [L = $HC(N^tBu)_2$], and ^{t}Bu-**5** [L = $HCO(N^tBu)$]. It was shown that for model catalysts **1**−**7** the barrier for chain initiation reaction is 11−21 kcal/mol. Reactant, π-complex, and product have either eclipsed or nearly untwisted ligands L, depending on the size of L−Zr ring, whereas the insertion transition state has the planes of the two ligands L twisted with respect to each other. Bulky substituents in catalysts ^{t}Bu-**4** and ^{t}Bu-**5** lead to a significant twisting of the ligands L in the reactant and π-complex while retaining the structure of the transition state. As a result, the π-complex is destabilized, and the insertion barrier is lowered by several kcal/mol. Among all catalysts studied, ^{t}Bu-**5** is expected to be best. It was also shown that polymerization catalyzed by these catalysts is likely to produce linear polyethylene.

Introduction

Polymerization of olefin catalyzed by soluble, single-site homogeneous catalysts has been a focus of studies in the last several decades because of its industrial importance.[1−3] Currently, there are two distinct trends in olefin polymerization studies. The first of them is the adjustment of ligand, cocatalyst, solvent, and metal for existing metallocene-based catalysts in an effort to improve their catalytic activity and polymer properties.[4] The second is the search for new and more active alternative catalysts. Recently, several effective alternative catalysts have been discovered. Among them are diimine-M(II) (M = Ni, Pd),[5] 2,6-bis(imino)pyridyl-M(II) (where M = Fe and Co),[6] Ti- and Zr-alkoxide,[7] Ti- and Zr-diamido,[8] and Al-based[9] catalysts.

Numerous studies have demonstrated the complexity of the catalyzed olefin polymerization, which is believed

† Present address: Arbeitsgruppe Quantenchemie, Institut für Chemie, Humboldt-Universität zu Berlin, Jägerstr. 10-11, D-10117 Berlin, Germany.

(1) For representative references, see: (a) Huang, J.; Rempel, G. L. *Prog. Polym. Sci.* **1995**, *20*, 459. (b) Coates, G. W.; Waymouth, R. M. *Science* **1995**, *267*, 217. (c) van der Linden, A.; Schaverien, C. J.; Meijboom, N.; Ganter, C.; Orpen, A. G. *J. Am. Chem. Soc.* **1995**, *117*, 3008. (d) Yang, X.; Stern, C. L.; Marks, T. J. *J. Am. Chem. Soc.* **1994**, *116*, 10015. (e) Coughlin, E. B.; Bercaw, J. E. *J. Am. Chem. Soc.* **1992**, *114*, 7606. (f) Crowther, D. J.; Baenziger, N. C.; Jordan, R. F. *J. Am. Chem. Soc.* **1991**, *113*, 1455. (g) Kaminsky, W.; Kulper, K.; Brintzinger, H. H.; Wild, F. R. W. P. *Angew. Chem., Int. Ed. Engl.* **1985**, *24*, 507. (h) Ewen, J. A. *J. Am. Chem. Soc.* **1984**, *106*, 6355. (i) Richardson, D. E.; Alameddin, N. G.; Ryan, M. F.; Hayes, Th.; Eyler, J. R.; Siedle, A. R. *J. Am. Chem. Soc.* **1996**, *118*, 11244. (j) Alameddin, N. G.; Ryan, M. F.; Eyler, J. R.; Siedle, A. R.; Richardson, D. E. *Organometallics* **1995**, *14*, 5005.

(2) For representative references, see: (a) Yoshida, T.; Koga, N.; Morokuma, K. *Organometallics* **1995**, *14*, 746. (b) Yoshida, T.; Koga, N.; Morokuma, K. *Organometallics* **1996**, *15*, 766. (c) Woo, T. K.; Fan, L.; Ziegler, T. *Organometallics* **1994**, *13*, 2252. (d) Fan, L.; Harrison, D.; Woo, T. K.; Ziegler, T. *Organometallics* **1995**, *14*, 2018. (e) Lohrenz, J. C. W.; Woo, T. K.; Ziegler, T. *J. Am. Chem. Soc.* **1995**, *117*, 12793. (f) Fan, L.; Harrison, D.; Deng, L.; Woo, T. K.; Swerhone, D.; Ziegler, T. *Can. J. Chem.* **1995**, *73*, 989. (g) Hyla-Kryspin, I.; Niu, S.; Gleiter, R. *Organometallics* **1995**, *14*, 964.

(3) Lohrenz, J. C. W.; Woo, T. K.; Fan, L.; Ziegler, T. *J. Organomet. Chem.* **1995**, *497*, 91.

(4) See: (a) Chen, E. Y.-X.; Marks, T. J. *Chem. Rev.* **2000**, *100*, 1391. (b) Ittel, S. D.; Johnson, L. K.; Brookhart, M. *Chem. Rev.* **2000**, *100*, 1169. (c) All other papers in: *Chem. Rev.* **2000**, *100*.

(5) (a) Johnson, L. K.; Killian, C. M.; Brookhart, M. *J. Am. Chem. Soc.* **1995**, *117*, 6414. (b) Tempel, D. J.; Johnson, L. K.; Huff, R. L.; White, P. S.; Brookhart, M. *J. Am. Chem. Soc.* **2000**, *122*, 6686.

(6) (a) Freemantle, M. *Chem. Eng. News* **1998**, Apr 13, pp 11−12. (b) Britovsek, G. J. P.; Gibson V. G.; Kimberley, B. S.; Maddox, P. J.; McTavish, S. J.; Solan, G. A.; White, A. J. P.; Williams, D. J. *Chem. Commun.* **1998**, *1998*, 849. (c) Small, B. L.; Brookhart, M.; Bennett, A. M. A. *J. Am. Chem. Soc.* **1998**, *120*, 4049. (d) Small, B. L.; Brookhart, M. *J. Am. Chem. Soc.* **1998**, *120*, 7143. (e) Britovsek, G. J. P.; Bruce, M.; Gibson, V. G.; Kimberley, B. S.; Maddox, P. J.; Mastroianni, S.; McTavish, S. J.; Redshaw, C.; Solan, G. A.; Stroemberg, S.; White, A. J. P.; Williams, D. J. *J. Am. Chem. Soc.* **1999**, *121*, 8728.

(7) (a) Schaverien, C. J.; van der Linden, A.; Orpen, A. G. *Polym. Prepr. (Am. Chem. Soc., Polym. Div.)* **1994**, *35*, 672. (b) van der Linden, A.; Schaverien, C. J.; Meijboom, N.; Ganter, C.; Orpen, A. G. *J. Am. Chem. Soc.* **1995**, *117*, 3008. (c) Scollard, J. D.; McConville, D. H. *J. Am. Chem. Soc.* **1996**, *118*, 10008. (d) Kakugo, M.; Miyatake, T.; Mizunuma, K. *Chem. Express* **1987**, *2*, 445. (e) Miyatake, T.; Mizunuma, K.; Seki, Y.; Kakugo, M. *Makromol. Chem., Rapid Commun.* **1989**, *10*, 349. (f) Miyatake, T.; Mizunuma, K.; Seki, Y.; Kakugo, M. *Makromol. Chem., Makromol Symp.* **1993**, *66*, 203.

10.1021/om000705+ CCC: $20.00
Publication on Web 12/09/2000

to be a multistep process and to involve the following elementary reactions:

1. Catalyst activation by cocatalysts such as methylalumoxane (MAO) or $B(C_6F_5)_3$.

$$L_nM(CH_3)_2 + MAO \rightarrow L_nM(CH_3)^+(MAO)^- \quad (1)$$

2. Polymer chain initiation, which is believed to proceed via the Cossée−Arlman mechanism:[10]

$$L_nM(CH_3)^+ + C_2H_4 \rightarrow \pi\text{-complex, } L_nM(CH_3)(C_2H_4)^+ \rightarrow \text{transition state (TS) for insertion} \rightarrow \gamma\text{-agostic } L_nM(C_2H_4CH_3)^+ \rightarrow \text{TS for rotation} \rightarrow \beta\text{-agostic } L_nM(C_2H_4CH_3)^+ \quad (2)$$

3. Polymer chain propagation reaction that includes the following:

a. back-side (*trans* to the β-agostic H) attack of the substrate to the transition metal center of β-$L_nM(C_2H_4Me)^+$, proceeding via the Cossée−Arlman mechanism to yield linear polyethylene:

$$\beta\text{-}L_nM(C_2H_4CH_3)^+ + C_2H_4 \rightarrow \text{back-side } \pi\text{-complex, } L_nM(C_2H_4CH_3)(C_2H_4)^+ \rightarrow \text{TS} \rightarrow \beta\text{-}L_nM(C_2H_4)(C_2H_4CH_3)^+ \quad (3)$$

b. front-side (*cis* to β-agostic H) attack of the substrate to transition metal center of β-$L_nM(C_2H_4CH_3)^+$ to yield linear polyethylene:

$$\beta\text{-}L_nM(C_2H_4CH_3)^+ + C_2H_4 \rightarrow \text{front-side } \pi\text{-complex, } L_nM(C_2H_4CH_3)(C_2H_4)^+ \rightarrow \text{TS} \rightarrow \text{back-side } \pi\text{-complex, } L_nM(C_2H_4CH_3)(C_2H_4)^+ \rightarrow \text{TS} \rightarrow \beta\text{-}L_nM(C_4H_8CH_3)^+ \quad (4)$$

c. β-agostic C−H bond activation to form the metal hydrido-olefin complex $L_nM(H)(C_2H_3CH_3)^+$ with subsequent olefin rotation and reinsertion into the M−H bond, followed by substrate coordination to yield branched polyethylene:

$$\beta\text{-}L_nM(C_2H_4CH_3)^+ \rightarrow L_nM(H)(CH_2CHCH_3)^+ \rightarrow \text{rotation and reinsertion} \rightarrow L_nM(CH_3CHCH_3)^+ + C_2H_4 \rightarrow \text{branched polymer} \quad (5)$$

4. Typical polymer chain termination/transfer processes, β-H exchange between monomer and polymer and β-H elimination process, are as follows:

a. β-H exchange between monomer and polymer (BHExc) starts by front-side coordination of substrate to the transition metal center and proceeds via β-H transfer from polymer to monomer:

$$\beta\text{-}L_nM(C_2H_4CH_3)^+ + C_2H_4 \rightarrow \text{front-side } \pi\text{-complex, } L_nM(C_2H_4CH_3)(C_2H_4)^+ \rightarrow \text{TS for H-exchange} \rightarrow \beta\text{-}L_nM(CH_2CHCH_3)(C_2H_5)^+ \rightarrow L_nM(CH_2CHCH_3)(C_2H_5)^+ + CH_2CHCH_3 \quad (6)$$

b. β-Hydride elimination (BHElm), the first step of which is activation of the β-agostic C−H bond to form a hydrido-olefin complex $L_nM(CH_2CHCH_3)(H)^+$ that can dissociate into a olefin-terminating polymer and a hydrido complex L_nMH^+. The latter can initiate a new polymer chain:

$$L_nM(CH_2CH_2CH_3)^+ \rightarrow L_nM(CH_2CHCH_3)(H)^+ \rightarrow L_nMH^+ + CH_2CHCH_3 \quad (7)$$

Understanding the mechanism of these elementary reactions is extremely important and will allow us to search for new and more effective catalysts for olefin polymerization and control the structure of the polymers. In our previous papers we have theoretically studied the detailed mechanism of ethylene polymerization reactions catalyzed by the diimine-M(II) (M = Ni, Pd, and Pt)[11,12] and Ti- and Zr-alkoxide,[13,14] as well as 2,6-bis(imino)pyridyl-Fe(II) catalysts.[15] This paper is a continuation of our previous studies and deals with the mechanism of the $L_nZrCH_3^+$-catalyzed ethylene polymerization, where L is a non-cyclopentadienyl ligand such as carboxylate, amidinate, ketonate, and di(aza)ketonate. Here, our aim is to elucidate the role of electronic and steric effects and to obtain some guidance for designing new and more efficient catalysts. For all the active catalytic species given in Scheme 1, we examined the chain initiation reaction 2. For catalysts **3** and **4**, we additionally studied (i) the chain propagation leading to the linear polymer, reaction 3, (ii) chain branching, the first part of reaction 5, and (iii) BHEli reaction 7. To elucidate the role of bulky substituents as ancillary ligands, we also studied the *tert*-butyl-substituted species of **4** and **5**, ^{t}Bu-**4** and ^{t}Bu-**5**, respectively.

It should be noted that the olefin polymerization catalyzed by the non-Cp ligated Zr and Ti complexes, such as Zr{*N*,*N*′-bis(trimethylsilyl)-β-diketiminato}Cl_3,[16] $[ArN(CH_2)_3NAr]MR_2$ (M = Zr and Ti, Ar = 2,6-^{i}Pr$_2$C$_6$H$_3$,

(8) (a) Schrock, R. R.; Baumann, R.; Reid, S. M.; Goodman, J. T.; Stumpf, R.; Davis, W. M. *Organometallics* **1999**, *18*, 3649. (b) Baumann, R.; Stumpf, R.; Davis, W. M.; Liang, L.-C.; Schrock, R. R. *J. Am. Chem. Soc.* **1999**, *121*, 7822. (c) Liang, L.-C.; Schrock, R. R.; Davis, W. M.; McConville, D. H. *J. Am. Chem. Soc.* **1999**, *121*, 5797. (d) Aizenberg, M.; Turculet, L.; Davis, W. M.; Schattenmann, F.; Schrock, R. R. *Organometallics* **1998**, *17*, 4795. (e) Baumann, R.; Davis, W. M.; Schrock, R. R. *J. Am. Chem. Soc.* **1997**, *119*, 3830.

(9) Coles, M. P.; Jordan, R. F. *J. Am. Chem. Soc.* **1997**, *119*, 8125. (b) Ihara, E.; Young, V. G., Jr.; Jordan, R. F. *J. Am. Chem. Soc.* **1998**, *120*, 8277. (c) Radzewich, C. E.; Coles, M. P.; Jordan, R. F. *J. Am. Chem. Soc.* **1998**, *120*, 9384, and references therein.

(10) (a) Cossée, P. *J. Catal.* **1964**, *3*, 80. (b) Arlman, E. J.; Cossée, P. *J. Catal.* **1964**, *3*, 99.

(11) (a) Musaev, D. G.; Froese, R. D. J.; Svensson, M.; Morokuma, K. *J. Am. Chem. Soc.* **1997**, *119*, 367. (b) Musaev, D. G.; Froese, R. D. J.; Morokuma, K. *New J. Chem.* **1997**, *21*, 1269. (c) Musaev, D. G.; Svensson, M.; Morokuma, K.; Strömberg, S.; Zetterberg, K.; Siegbahn, P. E. M. *Organometallics* **1997**, *16*, 1933.

(12) (a) Froese, R. D. J.; Musaev, D. G.; Morokuma, K. *J. Am. Chem. Soc.* **1998**, *120*, 1581. (b) Musaev, D. G.; Froese, R. D. J.; Morokuma, K. *Organometallics* **1998**, *17*, 1850.

(13) Froese, R. D. J.; Musaev, D. G.; Matsubara, T.; Morokuma, K. *J. Am. Chem. Soc.* **1997**, *119*, 7190.

(14) Froese, R. D. J.; Musaev, D. G.; Morokuma, K. *Organometallics* **1999**, *18*, 373.

(15) Khoroshun, D. V.; Musaev, D. G.; Vreven, T.; Morokuma, K. Submitted for publication.

(16) (a) Hitchcock, P. B.; Lappert, M. F.; Liu, D.-S. *J. Chem. Soc., Chem. Commun.* **1994**, 1699. (b) Lappert, M. F.; Liu, D.-S. Neth. Pat. Appl. 9500085, 1985.

Scheme 1. Active Catalytic Species Modeled in this Paper

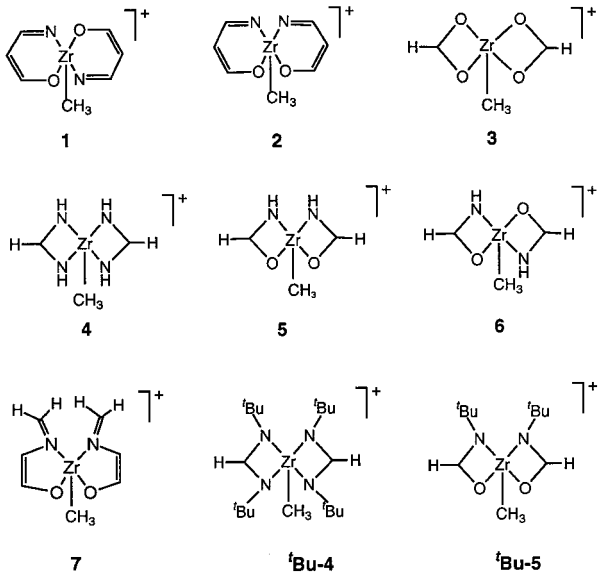

and R = Me and CH_2Ph),[17] and $[\eta^4$-4-$RC_6H_4C(NSiMe_3)_2]_2$-MCl_2 (R = H and CH_3) (M = Ti and Zr),[18] were the subject of several experimental studies. It was shown that these complexes demonstrate modest catalytic activities.

Computational Procedure

Geometries and energies of the reactants, intermediates, transition states, and products for catalysts **1**−**7** were calculated using the hybrid density functional B3LYP method[19] as implemented in the Gaussian94 package.[20] The standard valence-double-ζ LANL2DZ basis set[21] with the corresponding effective core potential (for Zr atom) was used for all the calculations. For *tert*-butyl-containing ^{t}Bu-**4** and ^{t}Bu-**5**, we employed the integrated molecular orbital−molecular mechanics (IMOMM) procedure.[22] This method has already been successfully used for olefin polymerization studies.[12,23] In this approach,[22,24] the energy of the system of interest, called "real system", is represented by a sum of quantum-chemical ("MO", i.e., B3LYP/LANL2DZ in our case) energy of a smaller "model system" and the molecular mechanical ("MM") energy of the real system. From the latter, all interactions accounted for by MO for the small system are excluded. The MM energy was calculated with the MM3 force fields. For the Zr atom, the van der Waals parameters reported by Rappé[25] were used. Calculations were carried out with the IMOMM program,[22] which makes use of the modified MM3(92)[26] and modified Gaussian 92/DFT[27] codes. All structures (both at pure B3LYP and IMOMM levels) were optimized without symmetry constraints. **4** and **5** were used as the model systems for ^{t}Bu-**4** and ^{t}Bu-**5**, respectively. The N−H distances in the model systems were fixed at 1.025 Å, and the N−C distances in the real systems were fixed at 1.49 Å.

Here one should note the following. (a) The energetics discussed below does not include zero-point vibrational energy and entropy corrections nor the solvent effects. Due to the large size of the systems, we could not perform vibrational analysis. However, the nature of the calculated transition states was confirm by "quasi-IRC" calculations. (b) The basis set used, LANL2DZ, is a standard basis set and was not augmented. As was shown previously, B3LYP/LANL2DZ approximation used in this paper describes the absolute barrier heights of similar systems with about 5−6 kcal/mol error.[28] Therefore, we will mainly pay attention to relative rather than absolute values and discuss qualitative trends.

Results and Discussions

1. Chain Initiation Reaction. As mentioned above, one of the important elementary reactions involved in the transition metal-catalyzed ethylene polymerization process is the polymer chain initiation reaction 2. It starts with the coordination of the substrate to the cationic transition metal complex (complex $L_2Zr(CH_3)^+$ in the present cases) to form an olefin−alkyl π-complex, followed by insertion of the substrate into the Zr−alkyl bond via a four-center transition state to form a γ-agostic Zr−alkyl complex. The latter rearranges easily to a more stable product, the β-agostic alkyl complex. This mechanism ignores the role of the counterion, (CH_3)(cocatalyst)$^-$, in the polymer chain initiation process, so we will study it without taking into account the counterion effect. Let us start our discussion with the geometries of the calculated reactants, transition states, intermediates, and products of reaction 2.

1.A. Geometries. Reactants. Calculated geometries of the reactants $L_2Zr(CH_3)^+$ with various ligands L are shown in Figures 1−3. Catalyst **1** and **2** contain two (O−CH=CH−CH=NH) ligands with *trans* and *cis* orienta-

(17) (a) Scollard, J. D.; McConville, D. H.; Payne, N. C.; Vittal, J. J. *Macromolecules* **1996**, 5241. (b) Guerin, F.; McConville, D. H.; Vittal, J. J. *Organometallics* **1995**, *14*, 3154. (c) Scollard, J. D.; McConville, D. H.; Vittal, J. J. *Organometallics* **1995**, *14*, 5478.

(18) (a) Herskovics-Korine, D.; Eisen, M. S. *J. Organomet. Chem.* **1995**, *503*, 307. (b) Flores, J. C.; Chien, J. C. W.; Rausch, M. D. *Organometallics* **1995**, *14*, 1827.

(19) (a) Becke, A. D. *Phys. Rev. A* **1988**, *38*, 3098. (b) Lee, C.; Yang, W.; Parr, R. G. *Phys. Rev. B* **1988**, *37*, 785. (c) Becke, A. D. *J. Chem. Phys.* **1993**, *98*, 5648.

(20) Frisch, M. J.; Trucks, G. W.; Schlegel, H. B.; Gill, P. M. W.; Johnson, B. G.; Robb, M. A.; Cheeseman, J. R.; Keith, T.; Petersson, G. A.; Montgomery, J. A.; Raghavachari, K.; Al-Laham, M. A.; Zakrzewski, V. G.; Ortiz, J. V.; Foresman, J. B.; Cioslowski, J.; Stefanov, B. B.; Nanayakkara, A.; Challacombe, M.; Peng, C. Y.; Ayala, P. Y.; Chen, W.; Wong, M. W.; Andres, J. L.; Replogle, E. S.; Gomperts, R.; Martin, R. L.; Fox, D. J.; Binkley, J. S.; Defrees, D. J.; Baker, J.; Stewart, J. J. P.; Head-Gordon, M.; Gonzalez, C.; Pople, J. A. *Gaussian 94*, revision D.3; Gaussian, Inc.: Pittsburgh, PA, 1995.

(21) Hay, P. J.; Wadt, W. R. *J. Chem. Phys.* **1985**, *82*, 270.

(22) Maseras, F.; Morokuma, K. *J. Comput. Chem.* **1995**, *16*, 1170.

(23) (a) Deng, L.; Margl, P.; Ziegler, T. *J. Am. Chem. Soc.* **1997**, *119*, 1094. (b) Deng L.; Woo, T. K.; Cavallo, L.; Margl, P. M.; Ziegler T. *J. Am. Chem. Soc.* **1997**, *119*, 6177.

(24) (a) Matsubara, T.; Maseras, F.; Koga, N.; Morokuma, K. *J. Phys. Chem.* **1996**, *100*, 2573. (b) Matsubara, T.; Sieber, S.; Morokuma, K. *Int. J. Quantum Chem.* **1996**, *60*, 1101. (c) Froese, R. D. J.; Morokuma, K. *Chem. Phys. Lett.* **1996**, *263*, 393.

(25) Rappé, A. K.; Casewit, C. J.; Colwell, K. S.; Goddard, W. A., III; Skiff, W. M. *J. Am. Chem. Soc.* **1992**, *114*, 1.

(26) MM3(92): Quantum Chemistry Program Exchange, Indiana University, 1992. Aped, A.; Allinger, N. L. *J. Am. Chem. Soc.* **1992**, *114*, 1.

(27) Frisch, M. J.; Trucks, G. W.; Schlegel, H. B.; Gill, P. M. W.; Johnson, B. G.; Wong, M. W.; Foresman, J. B.; Robb, M. A.; Head-Gordon, M.; Replogle, E. S.; Gomperts, R.; Andres, J. L.; Raghavachari, K.; Binkley, J. S.; Gonzalez, C.; Martin, R. L.; Fox, D. J.; Defrees, D. J.; Baker, J.; Stewart, J. J. P.; Pople, J. A. *Gaussian 92/DFT*, revision F.2; Gaussian, Inc.: Pittsburgh, PA, 1993.

(28) (a) Musaev, D. G.; Morokuma, K. *J. Phys. Chem.* **1996**, *100*, 6509. (b) Erikson, L. A.; Pettersson, L. G. M.; Siegbahn, P. E. M.; Wahlgren, U. *J. Chem. Phys.* **1995**, *102*, 872. (c) Ricca, A.; Bauschlicher, C. W., Jr. *J. Phys. Chem.* **1994**, *98*, 12899. (d) Heinemann, C.; Hertwig, R. H.; Wesendrup, R.; Koch, W.; Schwarz, H. *J. Am. Chem. Soc.* **1995**, *117*, 495. (e) Hertwig, R. H.; Hrusak, J.; Schroder, D.; Koch, W.; Schwarz, H. *Chem. Phys. Lett.* **1995**, *236*, 194. (f) Schroder, D.; Hrusak, J.; Hertwig, R. H.; Koch, W.; Schwerdtfeger, P.; Schwarz, H. *Organometallics* **1995**, *14*, 312. (g) Fiedler, A.; Schroder, D.; Shaik, S.; Schwarz, H. *J. Am. Chem. Soc.* **1994**, *116*, 10734. (h) Fan, L.; Ziegler, T. *J. Chem. Phys.* **1991**, *95*, 7401. (i) Berces, A.; Ziegler, T.; Fan, L. *J. Phys. Chem.* **1994**, *98*, 1584. (j) Lyne, P. D.; Mingos, D. M. P.; Ziegler, T.; Downs, A. J. *Inorg. Chem.* **1993**, *32*, 4785. (k) Li, J.; Schreckenbach, G.; Ziegler, T. *J. Am. Chem. Soc.* **1995**, *117*, 486.

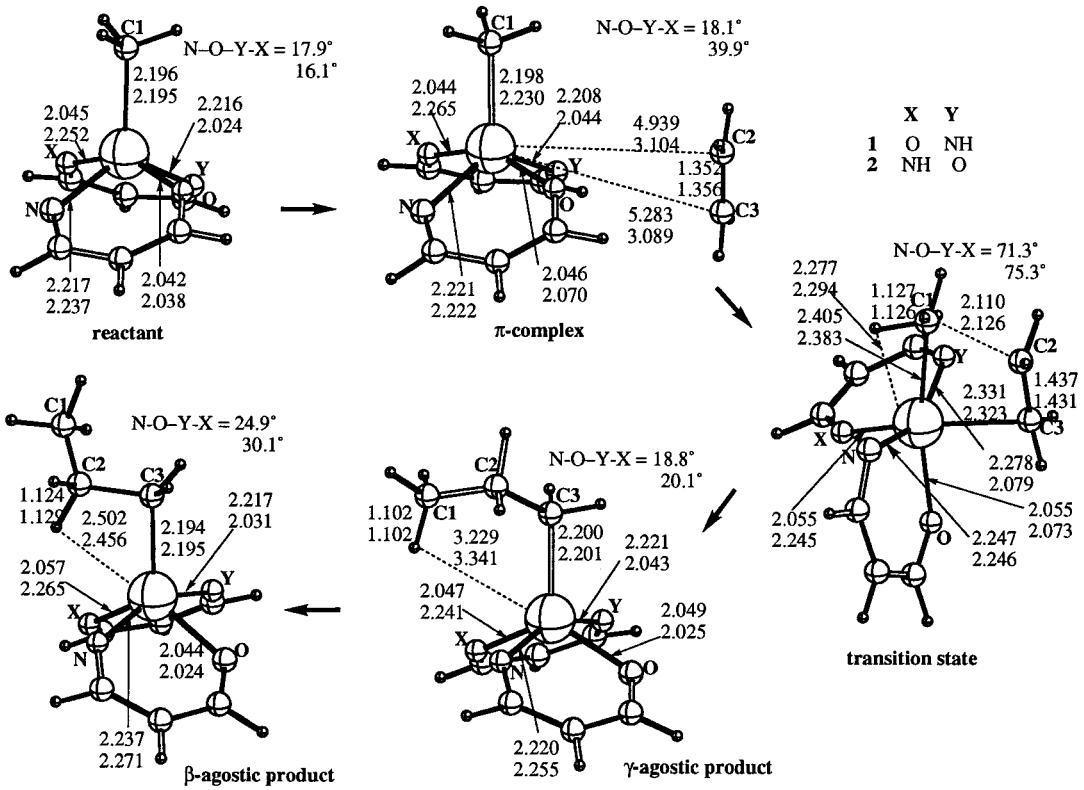

Figure 1. Optimized geometries (in Å) of reactant, π-complexes, transition state, and agostic products of the chain initiation step for catalysts **1** and **2**, with six-membered chelating rings. The perpendicular π-complex was found only for **2**.

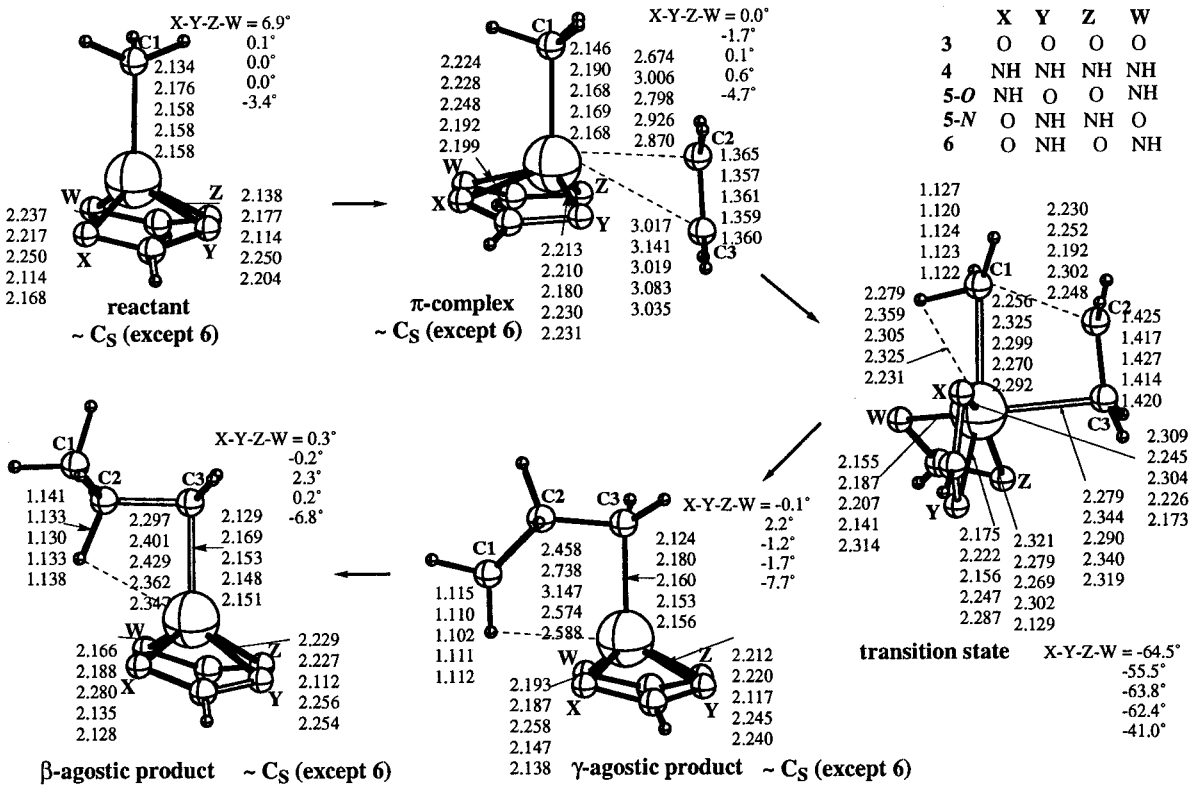

Figure 2. Optimized geometries (in Å) of reactant, π-complexes, transition state, and agostic products of the chain initiation step for catalysts **3**, **4**, **5** (*O*- and *N*-side attacks), and **6**, with four-membered chelating rings.

tion of the N atoms, respectively. Isomer **2** is calculated to be energetically 3.1 kcal/mol less stable than isomer **1**. As shown in Figure 1, they have a tetragonal-pyramidal structure with nearly planar six-membered zirconacycles. The ligands are slightly twisted relative to each other; the calculated twisting angles are 17.9° and 16.1° for **1** and **2**, respectively. In **1**, the bond distances for Zr−N and Zr−O are calculated to be about 2.217 and 2.045 Å, respectively, for both ligands L. However, for **2**, Zr−N distances are 2.252 and 2.237 Å,

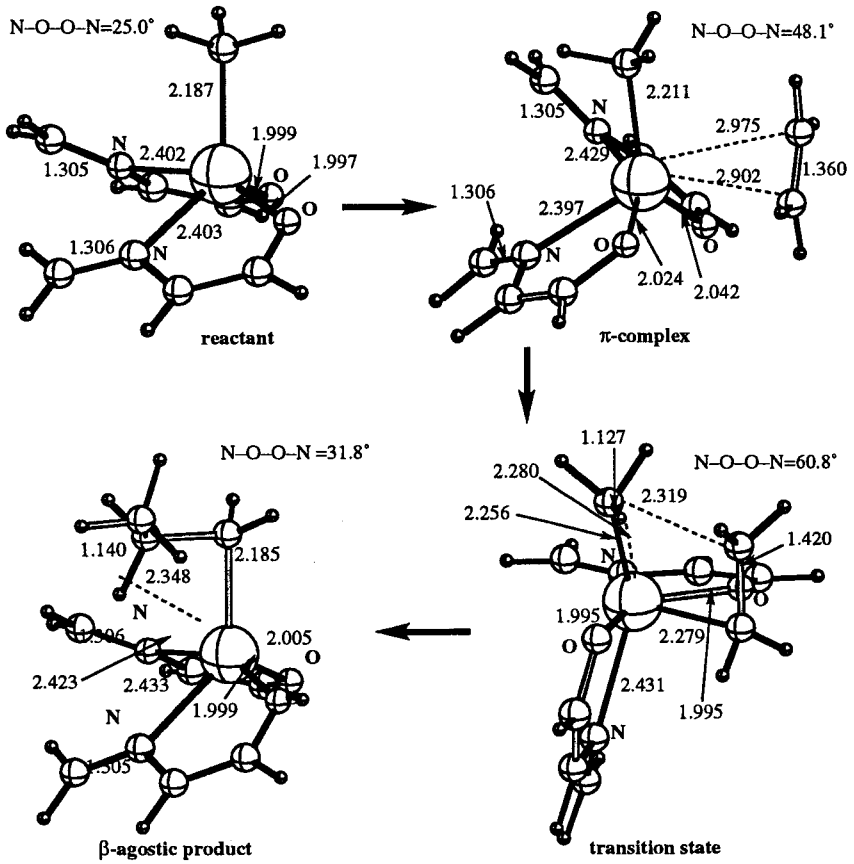

Figure 3. Optimized geometries (in Å) of reactant, π-complexes, transition state, and agostic products of the chain initiation step for catalyst **7**, with five-membered chelating rings. No γ-agostic product was found.

and Zr−O distances are 2.038 and 2.024 Å. A comparison of these numbers indicates that upon going from **1** to **2**, the Zr−N bond elongates by 0.04−0.02 Å, while the Zr−O bond shortens by 0.02 Å. This effect can be a result of the *trans* influence, indicating that in this case O is a stronger *trans* ligand than N.

The calculated geometrical parameters for catalysts **3**−**6** are given in Figure 2. Catalyst **3**, with two formate (L = HCO_2) ligands and four-membered zirconacycles, has a tetragonal-pyramidal structure with an apical methyl and overall C_s symmetry. The two formate ligands are not twisted relative to each other. Interestingly, the two Zr−O distances are substantially asymmetric within one formate; the Zr−O^1 bond, 2.237 Å, is 0.1 Å longer than the Zr−O^2 bond, 2.138 Å. Catalysts **4** and **5** with two amidate, (HN−CH−NH), and amidinate, (HN−CH−O), ligands, respectively, also possess C_s symmetry. In **4**, the Zr−N bond lengths within one ligand are 2.217 and 2.177 Å and differ by 0.04 Å. In **5**, the Zr−N bonds, which are oriented *cis* to each other are 2.250 Å, i.e., are longer than those in **4**. However, the Zr−O bond distances, which are also oriented *cis* to each other are 2.114 Å, i.e., shorter than those in **3**. Catalyst **6** is the *trans* isomer of **5** and is only 0.5 kcal/mol higher in energy than **5**. In this case the geometries of two amidinate ligands are slightly different, with Zr−O and Zr−N distances of 2.168, 2.204 and 2.108, 2.249 Å, respectively. There is no significant twisting of the amidinate ligands.

In catalyst **7**, with five-membered metallacycles, as shown Figure 3, the ligands preserve their planarity, as they do in **1** and **2**, while they are twisted with respect to each other. This result is similar to **1** and **2** and unlike **3**−**6**. The N−N−O−O dihedral angle of 25.0° for **7** is larger than that for **1** and **2**. The Zr−N bonds in **7**, 2.403 Å, are much longer than those in **1** and **2**. Consequently, its Zr−O bond length of 1.999 Å is much shorter than those in **1** and **2**.

In summary, the common features of the studied reactants are (i) pyramidal geometry with an apical methyl ligand; (ii) planar ancillary ligand rings; and (iii) ancillary ligands untwisted in three-membered ligands (**3**−**6**), but slightly twisted with respect to each other in four- and five-membered ligands (**1**, **2**, and **7**).

***π*-Complexes.** The $L_2ZrMe(\eta^2\text{-}C_2H_4)^+$ π-complex is the starting point of an important intermediate of the ethylene polymerization reactions. In general, one may expect two different π-complexes depending on the coordination mode of the incoming ethylene molecule: parallel and perpendicular, corresponding to the parallel and perpendicular positioning of the ethylene C−C bond with respect to the Zr−C^{Me} bond. In the case of **1**, the coordination of ethylene to the Zr center gives only a parallel π-complex; no perpendicular π-complex was found for this system. As seen in Figure 1, the calculated Zr−C_2H_4 bond distances are surprisingly long, about 5 Å, and the coordination of ethylene to the Zr-center of **1** does not change significantly the geometry of the reactant, except for slight elongation of the Zr−N and Zr−O bond distances, which obviously is a result of the interplay between L → Zr and C_2H_4 → Zr donations. Although the exact values of Zr−C_2H_4 bond distances may be inaccurate due to a limited performance of the B3LYP/LANL2DZ calculation at such long distances,

this result clearly indicates a very weak ethylene binding to this catalyst. The O−Zr−N bite angle increases only by 3° upon coordination of ethylene, and no additional twisting of the ligand rings relative to each other occurs.

The coordination of ethylene to catalyst **2** also gives only a parallel π-complex with much shorter Zr−C_2H_4 distances than that in **1**, but the distance is still longer than 3 Å, indicating a weak olefin−catalyst interaction. An important feature of this π-complex is that the substrate coordination significantly twists ligand rings. The dihedral N−N−O−O angle is calculated to be 39.9° in the π-complex, vs 16.1° in reactant **2**. This indicates a drastic difference in C_2H_4 interaction for **2** than for **1**, where the small twisting of ligands in the reactant (17.9°) remained unaltered in the π-complex (18.1°). The O−Zr−O bite angle in **2** (116°) is larger than in **1**, and there is less room for coordination of C_2H_4, which results in a deformation and twist of the ligands.

With a large bite angle in catalyst **3**, its parallel π-complex is not distorted and has C_s symmetry. This π-complex has much shorter Zr−$C^{ethylene}$ distances than those for **1** and **2**. The parallel π-complex for **4** has longer Zr−$C^{ethylene}$ bonds and a shorter C−C bond and hence is less strongly bound than for **3**. In the case of **5**, there are two sides (*N*-side and *O*-side, labeled as **5**-*N* and **5**-*O*, respectively) of the reactant available for coordination of the substrate, leading to two different π-complexes and, subsequently, to different transition states and products. For the *N*-side attack (**5**-*N*) of ethylene, the shortest $H^{ethylene}$−$H^{amidate}$ distance is only 2.59 Å in the π-complex, and the donative interactions and steric repulsion between the C_2H_4 and amidate ligands cause a large distortion of the ligands, with the N−Zr−N bite angle of 91.9° in the reactant becoming 132.3° in the π-complex vs from 117.3° to 131.6° in **3** and from 118.9° to 133.3° in **4**. For the *O*-side attack (**5**-*O*), the Zr−C_2H_4 bonds are shorter than for the *N*-side attack. Interestingly, the Zr−O ("*cis*") distances increase by 0.07 Å upon passing from the reactant to the π-complex, while the Zr−N ("*trans*") bond remains virtually unaltered. The π-complex of **6** is geometrically between those of **5**-*N* and **5**-*O*. Similarly to other species with three-membered rings, it has virtually untwisted ligand rings. No perpendicular π-complexes were found for the catalysts **3**−**6**.

For catalyst **7** we found only one π-complex. With the C^{Me}−Zr−$(C-C)^{ethylene}$ dihedral angle of 45.6°, it could be properly referred to neither as "parallel" nor as "perpendicular". Similar geometrical twist has been reported earlier for different transition metal complexes.[29] The ligands in the π-complex (with the dihedral N−N−O−O angle of 35.9°) are twisted more strongly than in the reactant (25.0°). The larger twisting is related to the increase in the O−Zr−O bite angle (from 109.1° in the reactant to 118.4° in the π-complex), which enables the CH_2 groups (from the ligand L) to come closer to each other. In the symmetric configuration with untwisted ligands (which is not a minimum and is 5.3 kcal/mol less stable than the twisted minimum), the H atoms of two CH_2 groups are only 1.996 Å apart, but in the asymmetric (energy minimum) configuration they are 3.199 Å apart from each other.

To sum up the results for the π-complexes, the Zr−$C^{ethylene}$ bond lengths vary widely depending on the ancillary ligand. The mutual twisting of the ancillary ligands depends crucially on the size of the ring; less twisting takes place for smaller, three-membered rings, where a larger bite angle leaves more room for the incoming ethylene. It increases by 11° for four-membered ligands in **1** (from 25° in reactant to 35.9° in π-complex), by 14° for five-membered ligands in **2** (from 16.1° to 39.9°), and by 18° (from 24.3° to 52.5°) for **7**.

Transition States. In this section we will discuss the geometries of the transition states corresponding to ethylene insertion into the Zr−Me bond from the parallel π-complexes. Since the olefin insertion into the Zr−alkyl bond is found to be one of the rate-determining steps of many olefin polymerization processes, we decided to investigate it in more detail.

In general, during the ethylene insertion into a Zr−Me bond, the metal−Me bond and π-bond of the ethylene molecule are broken and Me−ethylene(C^β−C^γ) and metal−C^α bonds are formed. As seen from Figures 1−3, the calculated geometries of the obtained transition states are consistent with this qualitative picture. Indeed, the broken Zr−Me(C^γ) and C^α−C^β bonds are elongated by 0.361 and 0.085 Å, for **1**, 0.128 and 0.075 Å for **2**, 0.110 and 0.060 Å for **3**, 0.135 and 0.060 Å for **4**, 0.131 and 0.067 Å for **5**-*O*, 0.101 and 0.055 Å for **5**-*N*, 0.124 and 0.060 Å for **6**, and 0.175 and 0.060 Å for **7**. On the other hand, the Zr−C^α and C^β−C^γ bonds to be formed are shortened and are 2.331 and 2.110 Å for **1**, 2.323 and 2.126 Å for **2**, 2.279 and 2.230 Å for **3**, 2.344 and 2.252 Å for **4**, 2.290 and 2.192 Å for **5**-*O*, 2.340 and 2.302 Å for catalyst **5**-*N*, 2.319 and 2.248 Å for **6**, and 2.279 and 2.319 Å for **7**. These geometry changes are typical for olefin insertion transition states.[30]

The ancillary ligands themselves also undergo significant changes. In the transition states, they are twisted so much that they become roughly perpendicular to each other. The twisting angle is calculated to be 70.3°, 64.0°, 55.5°, 53.3°, 63.8°, 41.0°, and 58.5° in **2**, **3**, **4**, **5**-*N*, **5**-*O*, **6**, and **7**, respectively. The Zr−O and especially the Zr−N distances become longer, but the ligand retains its planarity. The spectacular twisting of the ligands is apparently a result of a changing bonding environment during the reaction. More precisely, the Zr−C^α bond in the transition state has already acquired significant σ-bond character. Consequently, the transition state system turns to a true six-coordinated structure, which prefers an octahedral or nearly octahedral geometry. This causes the ligands to adopt the twisted configuration. Note that the reactant L_2ZrMe^+ and the products L_2ZrPr^+ (vide infra) are pentacoordinated complexes, while the π-complex should be better described as a pentacoordinated complex with an additional weakly bound ethylene ligand. In other words, during the reaction π-complex → TS → γ-complex, the metal center changes its coordination number from five → six → five, respectively.

Also, it should be noted that the transition states have a significant agostic bond character due to the methyl group. Indeed, Figures 1−3 show that one of the C−H

(29) See: Albright, T. A.; et al. *Orbital Interactions in Chemistry*; John Wiley & Sons: New York, 1997.

(30) Musaev, D. G.; Morokuma, K. *Top. Catal.* **1999**, *7*, 107.

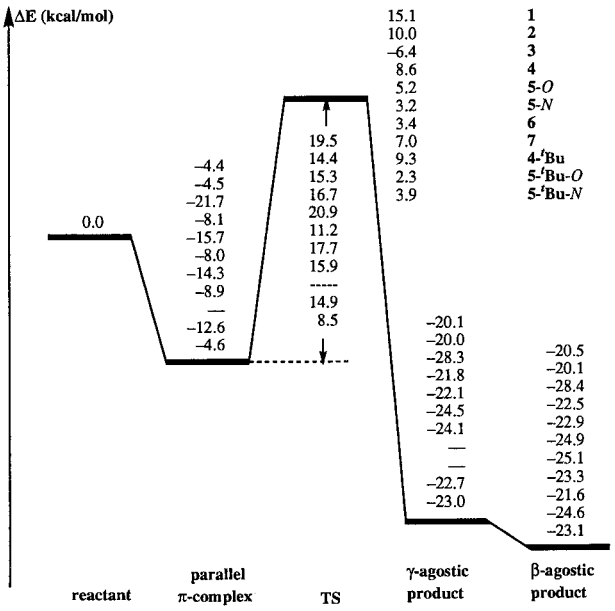

Figure 4. Potential energy profiles of the chain initiation step (reaction 2) for all the catalysts.

bonds of the methyl group is elongated as much as 0.04 Å because of the interaction with the Zr center.

Products: Agostic Complexes. The product of the ethylene insertion reaction is the propyl complex L_2ZrPr^+, which can contain either β- or γ-agostic interactions. The γ-agostic product is presumably formed first, with subsequent rearrangement to yield the β-agostic product. The strength of an agostic interaction can be roughly estimated on the basis of the $Zr-H^{agostic}$ and $C-H^{agostic}$ distances. In the γ-agostic products for **1** and **2**, the agostic bond is very weak, with a large $Zr-H^{agostic}$ distance, 3.229 and 3.341 Å, and a short $C-H^{agostic}$ bond 1.102 Å, respectively. The β-agostic products exhibit a much shorter $Zr-H^{agostic}$ distance (2.502 and 2.456 Å) and a longer $C-H^{agostic}$ bond (1.124 and 1.129 Å), respectively, than the γ-agostic product. In **3**−**6**, the γ- and β-agostic bonds in the products are stronger than those in **1** and **2**, which is illustrated by shorter $Zr-H^{agostic}$ separations and markedly elongated $C-H^{agostic}$ bonds.

Interestingly, in the γ- and β-agostic products, ancillary ligands are either nontwisted (which is the case for **3**−**6**) or twisted very little (which is the case for **1**, **2**, and **7**) relative to each other. Thus, in the reactant the twisting angle of the ancillary ligands is either zero (**3**−**6**) or small (**1**, **2**, and **7**). In the transition state the twisting angle increases dramatically and then decreases again in the β-agostic product to almost the same value as it was in the reactants.

For **7**, we were not able to locate any γ-agostic product, and it is not likely to exist; all optimization attempts led to the β-agostic product. In the β-agostic product, the agostic interaction is comparable to that of the corresponding three-membered ring species, **5**-*O*.

Note that we have not studied the transition state connecting γ- and β-agostic complexes because this reaction is not considered to be a rate-determining step or of chemical importance.

1.B. Energetics. As seen in Figure 4, we have presented the calculated energetics for the intermediates, transition states, and products of the reaction 2 for various model catalysts **1**−**7**. Of all the calculated π-complexes, those associated with **1** and **2** have the smallest ethylene binding energy of 4.4−4.5 kcal/mol, which is consistent with extremely long $Zr-C_2H_4$ bond distances in these complexes as discussed above. Their transition states are rather high in energy, 15.1 and 10.0 kcal/mol for **1** and **2** above the corresponding reactants. This is probably the consequence of the cost of geometry reorganization (mainly, the twisting of ligand rings) upon going from the π-complexes to the transition states. The calculated activation barriers (energy difference between the π-complex and corresponding transition state structures) are found to be 19.5 and 14.5 kcal/mol, respectively. This ~5 kcal/mol difference in the activation barriers is a result of the larger stability of the transition state for **2** compared to that for **1**. In accord with the weak agostic bonds in the products, the exothermicity of these two reactions is relatively small, about 20 kcal/mol. The β-agostic product is only slightly more stable than the corresponding γ-agostic product.

The π-complex for **3** has an ethylene binding energy of 21.7 kcal/mol. This is the most stable π-complex among all the systems under study. The high stability of the π-complex can be partially explained by the large bite angle of the formate ligands, which distort little upon coordination of ethylene. The transition state is significantly lower in energy than the reactant. However, the effects of a more stable π-complex and more stable transition state nearly cancel each other out, and the insertion barrier stays around 15.3 kcal/mol. The product of the reaction 2 for **3** is also more stable than those for all other catalysts studied here; the exothermicity of the reaction 2 for **3** is calculated to be 28.4 kcal/mol.

Although catalyst **4** is formally similar to **3**, it exhibits some quantitative differences. Most importantly, the ethylene binding energy of 8.1 kcal/mol, as well as the exothermicity of the reaction at 22.5 kcal/mol, is significantly less for **4** than for **3**. The reduced stability of the ethylene π-complex is in accord with the longer $Zr-C^{ethylene}$ bonds and shorter C−C bonds discussed above. The transition state for **4** is also less stable than that for **3** and lies 8.6 kcal/mol higher than reactants. However, the calculated insertion barrier, 16.7 kcal/mol, is very close to that for **3**.

For **5**-*N*, the π-complex is approximately as stable as that for **4**, and the transition state lies just 3.2 kcal/mol above the reactants, leading to an insertion barrier of 11.2 kcal/mol. The relative stability of the agostic products for this catalyst is between the corresponding values for **3** and **4**. The energetics for the *O*-side attack, **5**-*O*, is substantially different. The most important difference is that the π-complex is about twice as stable as for *N*-side attack. This is in accord with the $Zr-C^{ethylene}$ bond length, but apparently also contributed to by a smaller ligand distortion manifested by the change of the O−Zr−O bite angle from 118.7° to 130.4°. This transition state lies 2 kcal/mol higher than that for the *N*-side attack. Therefore, the insertion barrier is calculated to be 20.9 kcal/mol. The product of the reaction, L_2ZrPr^+, is also slightly more stable for *N*-side attack than for the *O*-side one. The comparison of these two pathways (*N*-side vs *O*-side) for catalyst **5** indicates that, while the *N*-side attack is kinetically more favorable, it

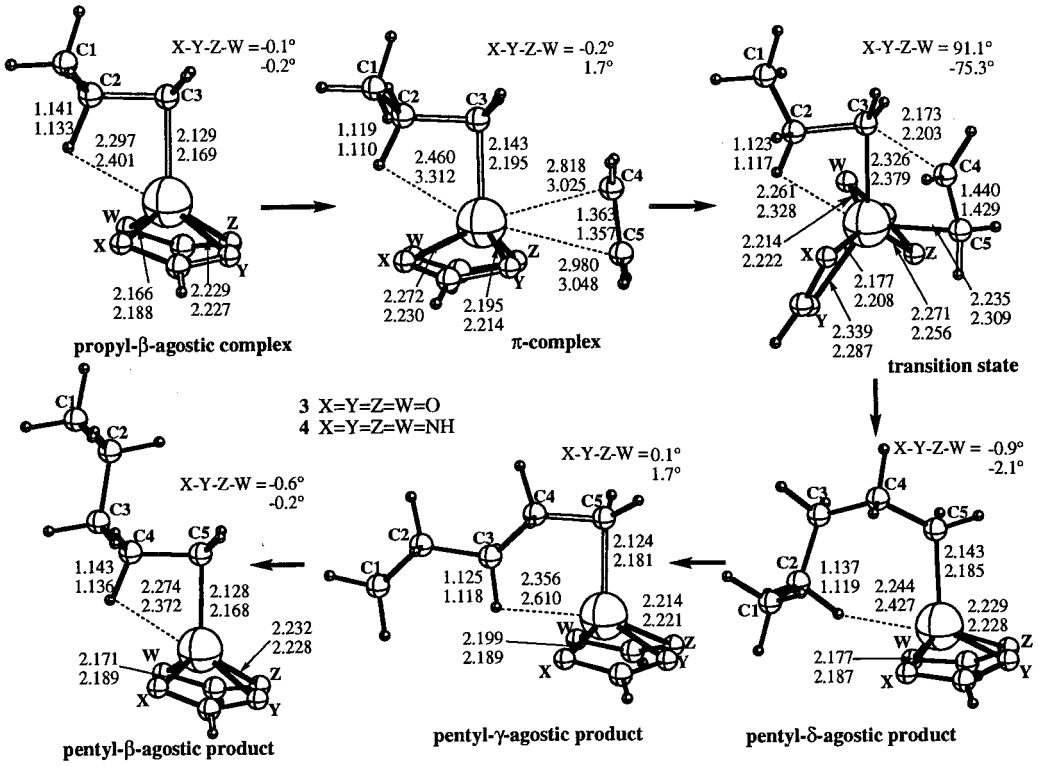

Figure 5. Optimized geometries (in Å) of reactant, π-complexes, transition state, and agostic products of the chain propagation step (back-side attack), reaction 3, for catalysts **3** (upper numbers) and **4** (lower numbers).

is thermodynamically not accessible because of a larger $L_2Zr(CH_3)^+-C_2H_4$ complexation energy on the *O*-side pathway. Therefore, the ethylene insertion into the Zr−Me bond of catalyst **5** is expected to be thermodynamically controlled. However, explicitly including solvent molecules and the zero-point energy and entropy corrections into calculations may change this situation (see our discussion below on catalyst ^{t}Bu-**5**-*O*).

The π-complex for **6** occupies an intermediate position between the **5**-*N*- and **5**-*O*-side, but is closer to the latter. The insertion barrier is calculated to be 17.6 kcal/mol for **6**. The overall exothermicity of the initiation step is, however, slightly larger for **6** than for both the **5**-*N*- and **5**-*O*-side. For **7**, which possesses four-membered rings, the ethylene complexation energy, insertion barrier, and overall exothermicity of reaction 2 are calculated to be 8.9, 15.9, and 23.3 kcal/mol, respectively.

Thus, the energetics of reaction 2 is substantially dependent upon the nature of the ancillary ligands L. In general, the ethylene insertion barriers are relatively high, 11−20 kcal/mol. In other words, if ethylene insertion into the Zr−Me bond is the rate-determining step of the ethylene polymerization process catalyzed by the studied model catalysts, one should expect a relatively slow polymerization. However, an exception can be the process proceeding via the *N*-side attack of the catalyst **5**, which shows the lowest insertion barrier (11.2 kcal/mol) of all studied systems.

2. Chain Propagation Reaction. As discussed above, the polymer chain propagation reactions (eqs 3−5) start from the product of the polymer chain initiation reaction, β-agostic alkyl complex. Below, we will discuss only reactions 3 and 4. Reactions 3 and 4 proceed via a mechanism similar to polymer chain initiation reaction 2 and lead to linear polymer. However, there are some important differences between reaction 2 and reactions 3 and 4. First, the reactant for the propagation reactions is a β-agostic complex, whereas the initiation step starts from a nonagostic Zr−methyl complex. Since some additional energy is required to destroy or weaken the agostic bond, the formed π-complex is expected to be less stable than that for the initiation step. Furthermore, while during the initiation reaction the coordination of C_2H_4 to the metal center from different positions is indistinguishable, during the chain propagation, a substrate can coordinate to the metal from two different sides; the two sides are the side of the agostic bond (front-side attack, reaction 4) and from the opposite side (back-side attack, reaction 3). This leads to two different processes. Indeed, the front-side attack implies a complete break of the agostic bond, because there is no room for both the agostic bond and the olefin ligand, and may lead either to polymer chain propagation via formation of a γ-agostic product or to chain transfer processes (see introduction to the paper). The back-side attack does not necessarily destroy the agostic bond completely, but usually it is weakened due to the *trans* effect of the olefin ligand. The back-side attack leads to polymer chain propagation via formation of a δ-agostic complex, which can further transform into γ- and β-agostic products. Taking into account the similarity in chain initiation and chain propagation steps, we studied reactions 3 and 4 only for catalysts **3** and **4**. The calculated geometries of reactants, intermediates, transition states, and products of back-side attack (eq 3) for **3** and **4** are presented in Figure 5, and those for front-side attack (eq 4) in Figure 6. The energetics are shown in Figure 7.

2.A. Catalyst 3. Back-side attack of the ethylene molecule to the catalyst **3** leads to formation of both the

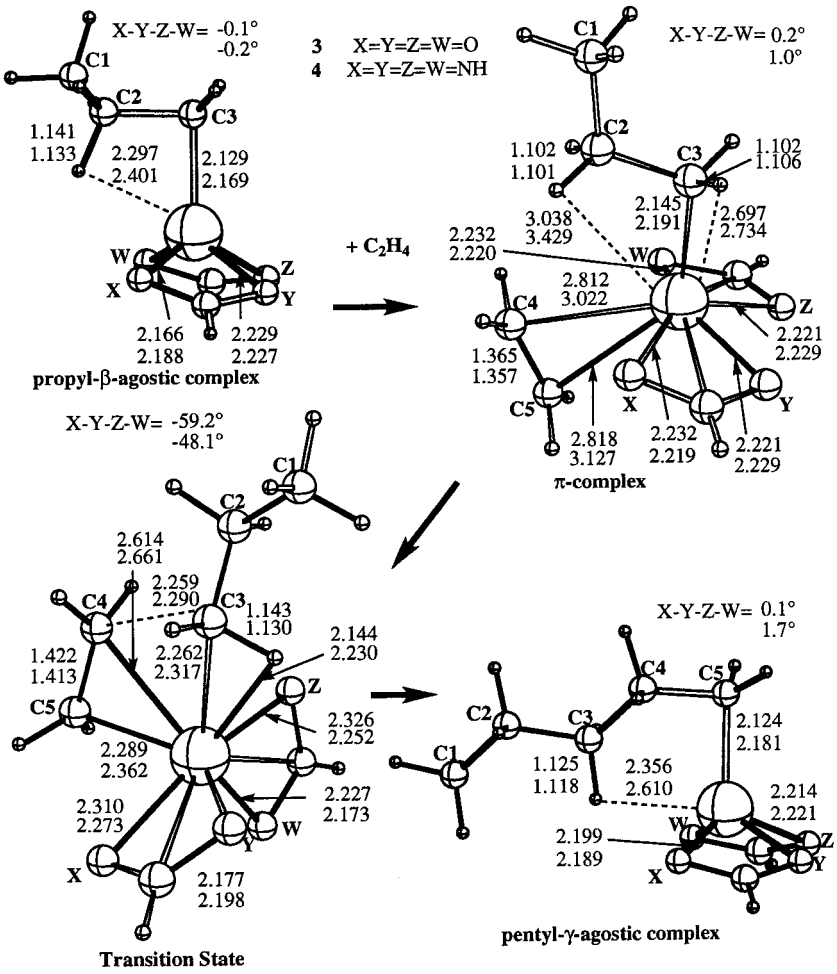

Figure 6. Optimized geometries (in Å) of reactant, π-complexes, transition state, and agostic products of the chain propagation step (front-side attack), reaction 4, for catalysts **3** (upper numbers) and **4** (lower numbers).

parallel and perpendicular π-complexes. However, the perpendicular π-complex, not shown in Figure 5, is calculated to be 5.2 kcal/mol less stable than the parallel one and will not be discussed in detail. As seen in Figure 5, the parallel π-complex retains the β-agostic bond, which is, however, elongated by 0.16 Å due to the *trans* effect of the C_2H_4 ligand. Compared to the initiation step, one of the Zr−C_2H_4 bonds is significantly longer, but the other is slightly shorter. In the parallel π-complex, the formate ligands are not twisted, with the O−O−O−O dihedral angle being −0.1°. The energetics, shown in Figure 7, indicate that the ethylene complexation energy of the parallel π-complex is 17.0 kcal/mol, which is 4 kcal/mol smaller than that for the initiation reaction in Figure 4.

The transition state for the propagation step shares the features of that for the chain initiation step, with the most important being the drastic twisting of the ligand. The agostic bond is preserved here and is even slightly shorter than in the β-agostic reactant. This agostic bond is reminiscent of a quite short δ-agostic bond, which is being formed. The transition state lies 5.5 kcal/mol below the β-agostic reactant. This value is quite close to the 6.4 kcal/mol for the initiation step. However, the destabilization of the π-complex (by about 4 kcal/mol) results in a decrease of the insertion barrier to 11.5 kcal/mol from 15.3 kcal/mol for the initiation step.

The primary product of reaction 3 is the δ-agostic complex, which lies 23.9 kcal/mol lower than reactants for **3**. However, it can easily transform to a more stable (by 1 kcal/mol) γ-agostic product. Surprisingly, its β-agostic product lies 1.4 kcal/mol higher in energy than the γ-agostic product. The overall exothermicity of the propagation reaction 3 is only 24.9 kcal/mol, which is 3.5 kcal/mol smaller than the corresponding value for the initiation step. This difference should be attributed to the agostic bond in the reactant of reaction 3.

Alternatively, the reaction can proceed via front-side attack, which is characterized by a completely broken β-agostic bond in the π-complex. As shown in Figure 6, in this case, only a parallel π-complex was located. It differs markedly from that for the initiation step. The Zr−C5 bond is much longer, most likely due to repulsion between the ethylene ligand and the ethyl group of the propyl ligand. This repulsion also accounts for a much more open C3−Zr−C5 angle. The elongation (and weakening) of the Zr−C5 bond is partly compensated by a shorter Zr−C4 bond. Finally, both Zr−$C^{ethylene}$ separations become almost equal. Overall, the front-side attack π-complex is only 0.7 kcal/mol less stable than that for back-side attack.

The transition state for front-side attack differs even more significantly from that for the back-side attack. Most importantly, both Zr−$C^{ethylene}$ bonds are much longer than in all the transition states described above.

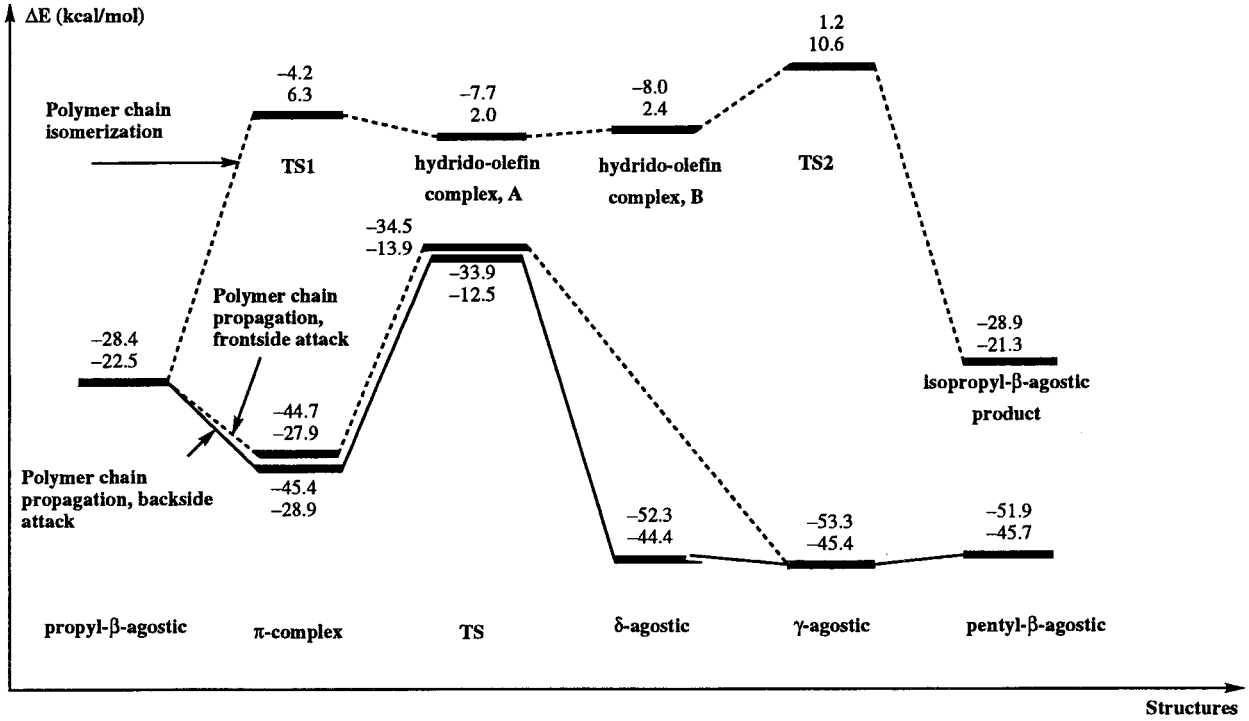

Figure 7. Potential energy profiles (in kcal/mol) for the polymer chain propagation (both back-side and front-side attacks) and polymer chain isomerization steps for catalysts **3** (upper numbers) and **4** (lower numbers). The energies are relative to the reactants: $L_2Zr(CH_3)^+ + C_2H_4$.

Interestingly, the Zr−C5 bond is even longer than in the π-complex. This means that the transition state is a rather early one. Accordingly, the C5−C6 bond is quite short and almost equal to that in the π-complex. Another peculiarity is a very large Zr−C1−C4 angle, which implies a substantial distortion of the propyl ligand. Similarly to the case of the front-side attack π-complex, all these geometrical features are easily explained by the repulsion between the propyl and ethylene ligands. Despite the fact that these structural features may be viewed as destabilizing, the energy of the front-side attack transition state is 0.6 kcal/mol lower than that of the back-side attack. The insertion barrier is 10.2 kcal/mol, i.e., the front-side attack is more preferable. However, the difference with the back-side attack is so small that it does not allow one to discriminate between the mechanisms. A very small difference was also reported for zirconocene catalysts, with the back-side attack being more favorable by about 0.3 kcal/mol[3]. Hence, both front- and back-side attack are predicted to take place. The front-side attack avoids the δ-agostic product and affords directly the γ-agostic product.

2.B. Catalyst 4. As shown in Figure 5 for the back-side attack in **4**, only a nontwisted parallel π-complex was found. Its geometry is very similar to that of the chain initiation step, with $Zr-C^{ethylene}$ bonds being only insignificantly longer than for the chain initiation step π-complex. The similarity is compounded by the absence of an agostic bond. Therefore, a relatively long and weak agostic bond in the β-agostic reactant vanishes completely in the π-complex due to the *trans* effect of the C_2H_4 ligand. The ethylene binding energy (6.4 kcal/mol), as shown in Figure 7, is somewhat smaller than that for the initiation step. This should be mainly attributed to the above-mentioned break of the β-agostic bond.

The transition state is again twisted with an N−N−N−N dihedral angle of 75.3°. The C3−C4 and Zr−C5 separations are smaller than the corresponding distances in the initiation step, while the C4−C5 bond is slightly longer. All these results indicate that this is a later transition state compared to the initiation step. An important feature of this transition state, which is shared also by **3**, is that a new short agostic bond is being formed corresponding to the δ-agostic bond in the product to be formed. The transition state is 10 kcal/mol above the β-agostic reactant, which corresponds to an activation energy of 16.4 kcal/mol. This is almost identical to the respective value for the initiation step.

The next participant of this reaction pathway is the δ-agostic complex. Its agostic bond is 0.18 Å longer than in the analogous δ-agostic complex for **3**. It is in accordance with the relatively weak β- and γ-agostic bonds. Similar to **3**, the agostic bonds in the β- and γ-agostic product are somewhat shorter than those for the initiation step. For **4**, the β-agostic product is the most stable one and is, therefore, the final product of the chain propagation reaction. The total exothermicity of the propagation step is 23.2 kcal/mol.

For the front-side attack of the substrate we have located a parallel π-complex as shown in Figure 6, which has slightly shorter $Zr-C^{ethylene}$ distances than that for the back-side attack, but much larger C3−Zr−C5 and Zr−C3−C4 angles. The front-side attack transition state differs drastically from that for **3**. The C1−C4 bond is only 2.290 Å. Though this value is markedly longer than for the back-side attack and for the initiation step, it is much shorter than in **3**. The $C^{ethylene}-C^{ethylene}$ bond is also close to that for the initiation step. The energy of this transition state is 1.4 kcal/mol lower than that of the back-side attack transition state. The activation

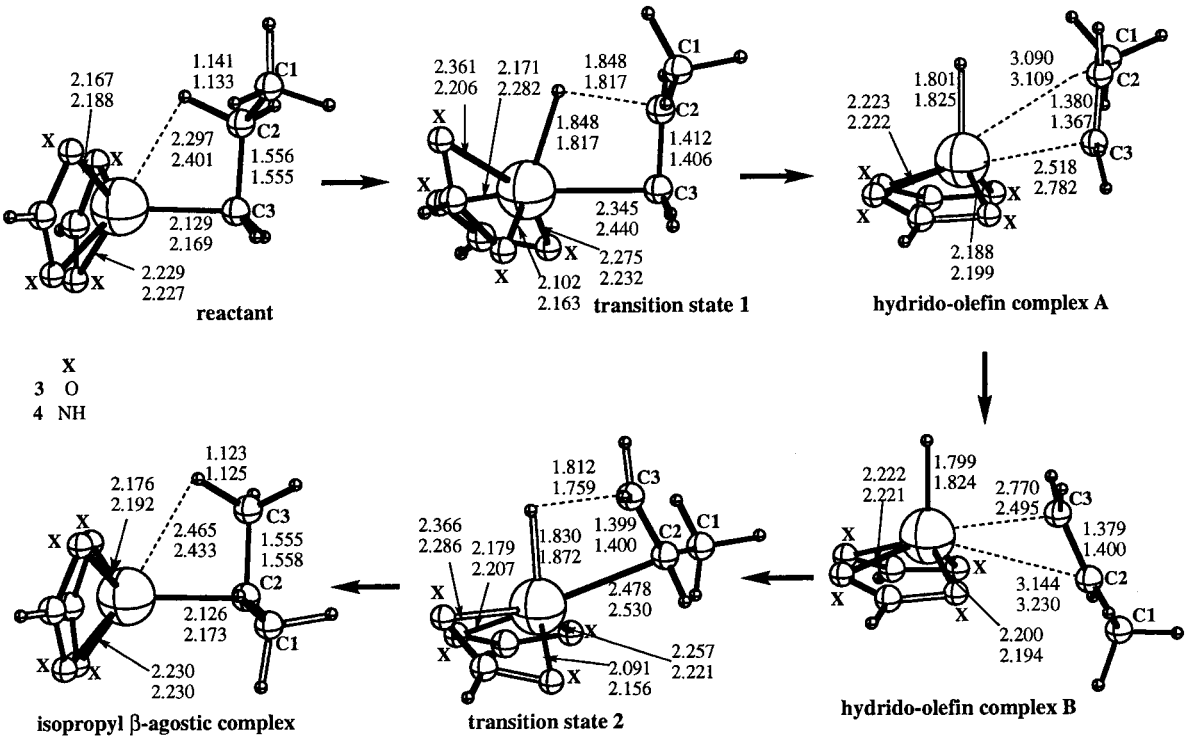

Figure 8. Optimized geometries (in Å) of reactant, π-complexes, transition state, and agostic products of the polymer chain isomerization step, reaction 5, for catalysts **3** (upper numbers) and **4** (lower numbers).

energy is 14.9 kcal/mol, which is 2.4 kcal/mol smaller than that for the back-side attack.

3. Chain Branching Reaction. The polymer chain branching reaction 5 can be divided into two steps. The first of them is polymer chain isomerization and starts with a β-agostic alkyl complex, proceeds via C−H bond activation and formation of a hydrido-olefin complex, $L_nM(H)(CH_2{=}CHCH_3)^+$, followed by an internal rotation of the olefin ligand and its reinsertion into the M−H bond to form $L_nM(CH(CH_3)_2)^+$. The second step is a polymer chain propagation process that starts with the substrate coordination to the $L_nM(CH(CH_3)_2)^+$ complex and yields branched polyethylene. Here, we study only the polymer chain isomerization process for the catalysts **3** and **4**, as shown in Figures7 and 8.

The geometries of the reactants, intermediates, transition states, and products of the polymer chain isomerization process for **3** and **4** are shown in Figure 8, and their relative energies in Figure 7. The hydrido-olefin complex, **A**, formed from the initial β-agostic propyl complex, is distinguished by a very asymmetric propene coordination, with two Zr−C distances differing by almost 0.6−0.5 Å. The Zr−H bond length of 1.8 Å is typical of zirconium hydride complexes. Energetically, this hydrido-olefin complex is 20.7 and 24.5 kcal/mol higher than the initial β-agostic complex for **3** and **4**, respectively. The transition state TS1 connecting this species with the corresponding reactant is rather late, with the Zr−H bond already formed, and is calculated to be 3.5 and 4.3 kcal/mol higher than the hydrido-propene complex, for **3** and **4**, respectively. The C−H bond activation energy is calculated to be 24.2 and 28.8 kcal/mol for **3** and **4**, respectively. Later, the hydrido-propene complex **A** transforms presumably easily to its isomer **B**, which lies only 0.3 kcal/mol lower for **3**, but 0.4 kcal/mol higher for **4**. This transformation might be described as an internal rotation about the Zr−C3 bond, which remains nearly unchanged.

Further isomerization of the hydrido-propene complex, **B**, to yield the isopropyl β-agostic complex proceeds via TS2. Geometrically, TS2 is similar to TS1 but is earlier in accord with the energetics. Energetically, TS2 is 5.4 and 4.3 kcal/mol less stable than TS1, for catalyst **3** and **4**, respectively. The activation energy for this step is found to be 9.2 and 8.2 kcal/mol, and the isopropyl β-agostic product lies only 0.5 kcal/mol lower and 1.2 kcal/mol higher than the reactants, for **3** and **4**.

Thus, polymer chain isomerization process that starts from the β-agostic propyl complex is an energetically unfavorable process because of higher agostic C−H bond activation barrier and low stability of the hydrido-olefin complex, **A**. It cannot compete with the polymer chain propagation, which has a much smaller, 11.5(10.2) and 16.4(14.0) kcal/mol, migratory insertion barrier (numbers in and without parentheses are for the back-side and front-side processes for **3** and **4**, respectively) and leads to linear polyethylene.

4. Effects of Bulky Substituents on the Reactivity and Reaction Mechanism. As seen from the above presented results for the polymer chain initiation reaction under study, (i) it occurs with a significant, 11.2−20.9 kcal/mol, insertion barrier, with the smallest barrier for catalyst **5**-*N*, and the largest for **5**-*O*; (ii) the ethylene coordination to the transition metal center gives only a parallel π-complex; (iii) the agostic product and π-complex have either eclipsed or only insignificantly twisted ligands L, whereas in the migratory insertions transition state (for every catalyst studied) the planes of the two ligands L are twisted with respect to each other in such a way that they form a quasi-octahedral environment for the Zr atom. In other words, the calculated transition state is additionally destabi-

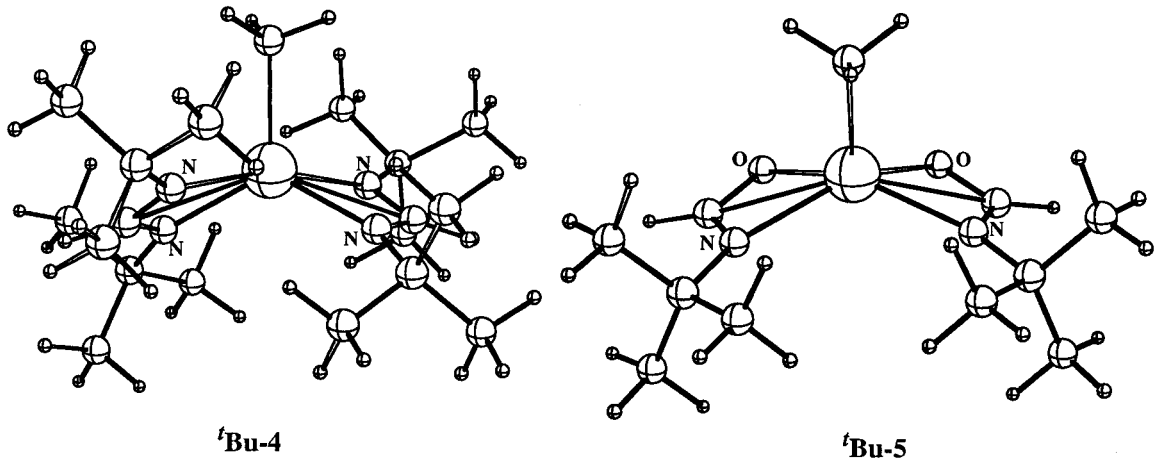

^{t}Bu-4 ^{t}Bu-5

Figure 9. IMOMM structures of the *tert*-butyl-substituted catalysts ^{t}Bu-**4** and ^{t}Bu-**5**. For clarity, the atoms in the ^{t}Bu-groups will not be shown in Figure 10.

lized because of twisting of the ligands L. Therefore, one can expect that a similar twisting of the ligands L in the corresponding reactant and π-complex (relative to which the insertion barrier is calculated) would decrease the migratory insertion barrier. One of the factors that could operate in this way might be steric effect. Bulky substituents at the ligands L can force the rings to be twisted in order to avoid the steric repulsion between the substituents. Note that a favorable influence of bulky substituents on the insertion barrier was recently predicted for a number of catalysts.[12,31]

To elucidate the role of the steric effects in the polymer chain initiation process studied above, we examined the chain initiation reaction for catalysts **4** and **5** with H atoms of the NH groups replaced by *tert*-butyl groups. These new catalysts are denoted as ^{t}Bu-**4** and ^{t}Bu-**5**, respectively. In these studies we have used the IMOMM method, integrating MO and MM methods (see section 2 for more detail).

4.A. Catalyst ^{t}Bu-4. For the chain initiation reaction for real catalyst ^{t}Bu-**4**, the IMOMM optimized geometry of the reactant is shown in Figure 9, and those of the reactant, π-complexes, transition states, and products are shown (omitting the ^{t}Bu group for clarity) in Figure 10. The reactant shows important geometrical differences in comparison with the model catalyst **4** shown in Figure 2; amidate ligands which are eclipsed in the model system **4** are strongly twisted in the real catalyst ^{t}Bu-**4**, with the N2−N1−N4−N3 dihedral angle of 36.5°. The geometry of the ligands L is rather asymmetric, with the Zr−N distances being different from each other. Except for Zr−N4, they are all longer than the respective bonds for the model catalyst **4**.

The structural changes in the π-complex, in comparing Figures 2 and 10, are more significant. First, the π-complex is a "perpendicular" one for the real catalyst ^{t}Bu-**4**, with a C^{methy}−Zr−C3−C2 dihedral angle of 74.4°, while for the unsubstituted catalyst **4** it was found to be parallel. Furthermore, the amidate ligands in the π-complex of ^{t}Bu-**4** are even more twisted than in the reactant; the N2−N1−N4−N3 dihedral angle is calculated to be 52.3° in the π-complex. This increase is due to a stronger steric repulsion. The two Zr−C_2H_4 bonds lengths differ more than they do in the model catalyst **4**. The Zr−N bond lengths differ significantly from those in model **4** π-complex. In other words, the π-complex of ^{t}Bu-**4** has a quasi-octahedral geometry.

The transition state for real catalyst ^{t}Bu-**4** reveals more similarity with its unsubstituted **4** homologue. The emerging C1−C3 bond is somewhat shorter for ^{t}Bu-**4**, but Zr−C2 is almost the same. More importantly, in the ^{t}Bu-**4** transition state the ligands L are twisted like in the model catalyst **4**. The N1−N2−N4−N3 dihedral angle in ^{t}Bu-**4** is 60.7°, which manifests little additional twisting in comparison to 55.5° in **4**. Note that the relative similarity of the real ^{t}Bu-**4** and the model **4** at the transition state is in agreement with our qualitative consideration (vide supra).

As we have seen before, chain initiation generally yields a γ-agostic product that can further transform to give a β-agostic product. However, in ^{t}Bu-**4**, all optimization attempts led to the β-agostic product and we were not able to locate any γ-agostic product; we conclude that it is does not exist. The β-agostic product is essentially similar to the reactant, with amidate rings twisted by 37.6°. The β-agostic product of the real catalyst ^{t}Bu-**4** has a 0.17 Å longer agostic bond compared to the model catalyst **4**. This is merely a result of the steric repulsion between the ^{t}Bu groups and the agostic hydrogen atom.

Within the context of the present study, the energetic changes caused by the ^{t}Bu substituents are even more important than their influence on geometry. The most important energy results for the chain initiation reaction 2 with real catalyst ^{t}Bu-**4** and model catalyst **4** are given in Table 1. Again, the IMOMM energy is the sum of the energy of the MO part and the energy of the MM part.

The most important difference between the model and the real systems is in the stability of the π-complexes. The real ^{t}Bu-**4** binds with ethylene weakly with the coordination energy of 2.4 kcal/mol, which is smaller by 5.7 kcal/mol than that for model **4**. The transition state of the real system is destabilized only by 0.7 kcal/mol with respect to that for the model system. As a result, the barrier for ethylene insertion falls to 11.7 kcal/mol in the real catalyst ^{t}Bu-**4** from 16.7 kcal/mol for the

(31) (a) Margl, P.; Deng, L.; Ziegler, T. *J. Am. Chem. Soc.* **1998**, *120*, 5517. (b) Margl, P.; Deng, L.; Ziegler, T. *J. Am. Chem. Soc.* **1998**, *120*, 5517.

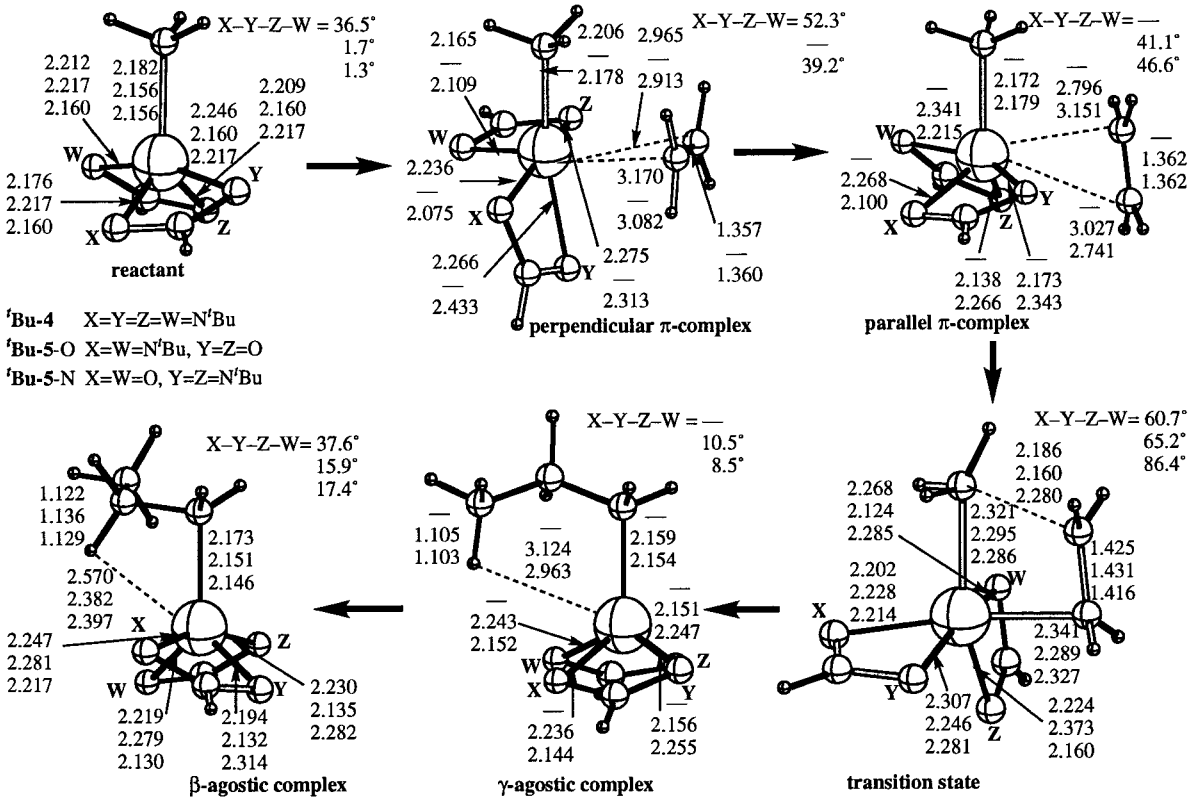

Figure 10. IMOMM optimized geometries (in Å) of reactant, π-complexes, transition state, and agostic products of the chain initiation step for *tert*-butyl-substituted catalysts ^{t}Bu-**4** and ^{t}Bu-**5** (both for *O*-side attack and *N*-side attack). For clarity, the atoms in the ^{t}Bu-groups are not shown.

Table 1. Relative Energies (in kcal/mol) for the Polymer Chain Initiation Reaction 2 for the Model 4 and Real ^{t}Bu-4 Systems

	model	real		
structures	MO	IMOMM = MO part + MM part		
reactant + ethylene	0.0	0.0	0.0	0.0
π-complex	−8.1	−2.4	−3.1	+0.7
transition state	+8.6	+9.3	+8.0	+1.3
γ-agostic *n*-propyl	−21.8			
β-agostic *n*-propyl	−22.5	−21.6	−21.6	0.0

model catalysts **4**. The β-agostic product is only slightly destabilized (by 0.9 kcal/mol) compared to the model system.

Even a cursory examination of the righthand column of Table 1 shows that the MM contribution, which is essentially the steric interaction, varies little going from reactant though π-complex and transition state to product. Thus, it is not the steric energy itself that contributes crucially to the total energy and leads to the decrease of the barrier. The obtained substantial difference between the model and the real systems is mainly contributed by the electronic effects or the energy change of the MO part due to the existence of the bulky substituents. In other words, the influence of the bulky substituents is indirect; the steric effects dramatically distort the geometry of the π-complex of the real system and induce large changes in the electronic energies.

To sum up, the steric interaction imposes a more substantial energy change on the π-complex than on the transition state and results in the decrease of the ethylene insertion barrier and improves the catalytic activity of the system.

4.B. Catalyst ^{t}Bu-5. As was discussed above, the incoming substrate may coordinate to the transition metal center of the model catalyst **5** via two different directions: from the side where two O-ligands are positioned (**5**-*O*), and from the side where two NH ligands are positioned (**5**-*N*). The **5**-*O* path proceeds through a relatively large, 20.9 kcal/mol, rate-determining barrier, while the second path, **5**-*N*, proceeds only through a 11.2 kcal/mol insertion barrier, which is found to be the lowest ethylene insertion barrier of all the studied model catalysts. Therefore, the examination of the polymer chain initiation reaction for the catalyst ^{t}Bu-**5** is of particular interest. The calculated geometries of the reactant, π-complexes, transition state, and products are shown in Figures 9 and 10.

Contrary to catalyst **4**, the differences between the substituted and unsubstituted reactants are relatively small in the case of catalyst **5**. Most importantly, the bulky alkyl groups cause no substantial amidinate ligand twisting, the N−O−O−N dihedral angle being only 1.3−1.7°. Obviously, the steric repulsion of two ^{t}Bu groups (as opposed to four in the case of catalyst ^{t}Bu-**4**) is not sufficient to distort the intrinsically eclipsed conformation of the ligands L. However, the presence of the bulky groups shortens the Zr−N bonds and elongates the Zr−O bonds. These changes can be a result of a significant increase in the N−Zr−N angle (122.8° in real catalyst ^{t}Bu-**5** compared to 91.9° in model catalyst **5**) and corresponding decrease in the O−Zr−O angle, which results in the decrease of the *trans* influence to N atoms from O atoms.

Let us start our discussions from the *O*-side attack. The π-complex experienced more significant changes

Table 2. Relative Energies (in kcal/mol) for the Polymer Chain Initiation Reaction 2 for the Model 5-*O* and Real ^{t}Bu-5-*O* Systems Proceeding via *O*-Side Coordination of Ethylene

	model	real		
structures	MO	IMOMM = MO part + MM part		
reactant + ethylene	0.0	0.0	0.0	0.0
π-complex	−15.7	−12.6	−14.5	+1.9
transition state	+5.2	+2.3	+2.2	+0.1
γ-agostic *n*-propyl	−22.1	−22.7	−22.7	0.0
β-agostic *n*-propyl	−22.9	−24.6	−24.7	+0.1

upon ^{t}Bu substitution than the reactant; the twisting of the imidinate ligands is strong, which is manifested by the N−O−O−N dihedral angle of 41.1°. However, the ligand twisting in the transition state, 65.2°, is close to that for the unsubstituted system, 63.8°. Both the γ-agostic and the β-agostic products are relatively similar to their respective model system homologues and will not be discussed in more detail. Thus, the replacement of the H atoms of NH groups with the ^{t}Bu groups in the catalyst **5**-*O* introduces a small distortion in the geometries of the reactant, product, and transition state of the polymer chain initiation reaction, whereas the π-complex experiences a large ligand twisting. Therefore, one should expect some destabilization of the π-complex of the real catalyst ^{t}Bu-**5**-*O* relative to reactant and transition state compared with those for model catalyst **5**-*O*. The calculated relative energies are shown in Table 2. Indeed, upon the substitution of the H atoms by ^{t}Bu groups, the π-complex is destabilized by 3.1 kcal/mol. At same time, the transition state for the real system ^{t}Bu-**5**-*O* is stabilized with respect to the reactant by 2.9 kcal/mol in comparison to the model system **5**-*O*. The overall effect of the transition state stabilization and the π-complex destabilization is the decrease in the ethylene insertion barrier by 6.0 kcal/mol, from 20.9 in the model system to 14.9 kcal/mol in the real system. In other words, these data unambiguously indicate that bulky substituents at nitrogen facilitate the olefin insertion into the Zr−alkyl bond. Table 2 indicates that the direct contribution from the MM interactions to the relative energy is extremely small, with an exception of the π-complex; the MM energy contributes only 1.8 kcal/mol to the total decrease in the activation energy. In other words, the steric interactions act mainly by means of induced indirect electronic effects, as is the case for the catalyst ^{t}Bu-**4**.

Let us now study the most promising path, ^{t}Bu-**5**-*N*, corresponding to the *N*-side attack of the substrate. Note that both a parallel and a perpendicular π-complex were located. Although the perpendicular π-complex is calculated to be 0.8 kcal/mol more stable than the parallel one, we will not discuss it here because the activation barrier, which is of primary interest, is the energy difference between the transition state and the parallel π-complex from which the reaction starts. As seen in Figure 10, the parallel π-complex is not a truly parallel one because the C1−Zr−C3−C2 dihedral angle is 26.9°. Some other geometrical parameters are also very different from its homologue for model catalyst **5**-*N*. First, it is extremely twisted, with an N−O−O−N dihedral angle of 46.6°. Second, the two Zr−C_2H_4 bonds are very different, with the Zr−C3 distance being much shorter than the Zr−C2 distance, opposite of the situation in **5**-*N*. On the other hand, the Zr−N1 bond is 0.17 Å longer in ^{t}Bu-**5**-*N* than in **5**-*N*.

Table 3. Relative Energies (in kcal/mol) for the Polymer Chain Initiation Reaction 2 for the Model 5-*N* and Real ^{t}Bu-5-*N* Systems, Proceeding via *N*-Side Coordination of Ethylene

	model	real		
structures	MO	IMOMM = MO part + MM part		
reactant + ethylene	0.0	0.0	0.0	0.0
perpendicular π-complex		−5.4	−5.6	+0.2
parallel π-complex	−8.0	−4.6	−4.7	+0.1
transition state	+3.2	+3.9	+3.4	+0.5
γ-agostic *n*-propyl	−24.5	−23.0	−23.7	+0.7
β-agostic *n*-propyl	−24.9	−23.1	−25.4	+2.3

The geometries of the transition state for the real and model systems are found to be rather similar. Similarly, the changes in the geometries of the agostic products of this reaction resemble those in the reactant, with the exception of a slightly longer agostic bond in ^{t}Bu-**5**-*N* than in **5**-***N***. The Zr−$H^{agostic}$ distance in the γ-agostic product is larger by almost 0.4 Å in the real system than in the model system.

The relative energies of the chain initiation reaction for the *N*-side attack are summarized in Table 3. As seen in this table, the relative stability of the parallel π-complex for ^{t}Bu-**5**-*N* is 3.4 kcal/mol smaller than that for **5**-*N*. The transition state is in this case only slightly (0.7 kcal/mol) destabilized by the steric effects. As a result, the steric effects decrease the migratory insertion barrier by 2.7 kcal/mol, from 11.2 in the model system to 8.5 kcal/mol for the real system. This 8.5 kcal/mol barrier for the real catalyst ^{t}Bu-**5**-*N* is small, and the polymer chain initiation reaction (and propagation as well) for this system should occur in very mild conditions, which could make catalyst ^{t}Bu-**5**-*N* of practical significance. However, the problem inherent in the model catalyst **5** remains for the real catalyst ^{t}Bu-**5**; the path ^{t}Bu-**5**-*O* corresponding to the ethylene *O*-side attack is thermodynamically more feasible because of the relatively large ethylene complexation energy of 12.6 kcal/mol, while it is kinetically less favorable because of the relatively large, 14.9 kcal/mol, migratory insertion barrier. The ethylene *N*-side attack path ^{t}Bu-**5**-*N* is thermodynamically less feasible because of a relatively small ethylene complexation energy of 4.6 kcal/mol, while it is kinetically more favorable because of a relatively small insertion barrier of 8.5 kcal/mol. In other words, if the reaction is thermodynamically controlled, it should proceed via the path ^{t}Bu-**5**-*O* and is expected to be a slow process. On the other hand, if reaction is controlled to proceed via thermodynamically less favorable path ^{t}Bu-**5**-*N*, then it is expected to be a relatively fast process.

However, one should note that the results presented in Tables 2 and 3 and discussed above do not include (i) zero-point energy and entropy corrections to the energy, which were shown to destabilize the π-complex and transition state about 10 kcal/mol relative to the reactants, and (ii) solvent effects, which (a) may completely block the kinetically unfavorable path ^{t}Bu-**5**-*O* because complexation of solvent molecule to the *O*-side complexation is expected to be stronger than the *N*-side, and (b) may additionally destabilize the π-complex and transition state relative to the unsaturated reactant.

Both of these effects are not likely to significantly change the energy difference between the π-complex and transition state.

Conclusions

From the discussions given above, several important conclusions may be drawn.

(1) The studied model complexes L_2ZrMe^+ are predicted to exhibit a moderate activity in ethylene insertion into the $Zr-CH_3$ bond, with the ethylene insertion barrier varying from 11 to 21 kcal/mol depending on the ligand L. The lowest barrier was found for catalyst **5** in the case of the *N*-side coordination of ethylene to the Zr-center. Ethylene insertion into $Zr-C_3H_7$ for propagation was studied only for catalysts **3** and **4** and is found to be 5−6 kcal/mol more favorable than that into $Zr-CH_3$ for initiation.

(2) The polymer chain branching process that starts from the β-agostic propyl complex is an energetically unfavorable process because of the high β-agostic C−H bond activation barrier (24 kcal/mol for **3** and 29 kcal/mol for **4**) and low stability of the hydrido-olefin complex. It cannot compete with polymer chain propagation starting from the same β-agostic propyl complex that occurs with a much smaller migratory insertion barrier (10 and 14 kcal/mol for **3** and **4**, respectively). Thus, ethylene polymerization catalyzed by the present model complexes $L_2Zr(CH_3)^+$ would produce only linear polyethylene.

(3) The reactants, π-complexes, and agostic products have either eclipsed or only insignificantly twisted ancillary ligands L, depending on the size of the L−M ring, whereas in all migratory insertion transition states the planes of the two ligands L are twisted with respect to each other in such a way as to form a quasi-octahedral environment for the Zr atom. Thus, the calculated transition states are additionally destabilized because of twisting of the ligands L. Therefore, one can expect that the similar twisting of the ligands L in the corresponding reactants and π-complexes (relative to which insertion barriers are calculated) would decrease the migratory insertion barriers.

(4) Indeed, IMOMM calculations of the real catalysts ^{t}Bu-**4** and ^{t}Bu-**5** show that the steric effects caused by bulky substituents significantly change the geometry of the π-complexes while retaining the structure of the transition state. As a result, the π-complex is destabilized with respect to the transition state, and the insertion barrier is lowered by 5, 6, and 3 kcal/mol for catalysts **4**, **5**-*O*-side attack, and **5**-*N*-side attack, respectively. Thus, the presence of bulky substituents at the ligands L increases the catalytic activity of **4** and **5**. The effect of bulky substituents on the transition states can be used for design of better catalysts by exploiting steric effects.

(5) Among all the studied reactions, the process ^{t}Bu-**5**-*N* corresponding to ethylene coordination from the *N*-side of the real catalyst ^{t}Bu-**5** is the most promising. If reaction is controlled kinetically, catalyst ^{t}Bu-**5** is expected to follow the ^{t}Bu-**5**-*N* pathway with high activity.

Acknowledgment. The present research is in part supported by a grant (CHE96-27775) from the National Science Foundation. Computer time allocated at the Emerson Center for Scientific Computation of Emory University, the Center for Supercomputing Applications (NCSA), and Maui High Performance Computer Center (MHPCC) is acknowledged.

OM000705+